Proceedings of ASME Turbo Expo 2011
GT2011
June 6-10, 2011, Vancouver, British Columbia, Canada

GT2011-46096

An Experimental Study of Lean Blowout with Hydrogen Enriched Fuels in a Swirl Stabilized Premixed Combustor

Shengrong Zhu, Sumanta Acharya

Turbine Innovation and Energy Research (TIER) Center
Department of Mechanical Engineering
Louisiana State University
Baton Rouge, LA 70803

ABSTRACT

Lean premixed combustion is widely used to achieve better compromise between nitric oxide (NOx) emissions and combustion efficiency (related to CO levels). However, combustor operation near the lean blowout (LBO) limit can render the flame unstable and lead to oscillations, flashback or extinction, thereby limiting the potential of lean combustion application. Recent interest in integrated gasification combined cycle plants (IGCC) and syngas combustion requires an improved understanding of the role of hydrogen on the combustion process. Therefore, in the present study, combustion of pure methane and blended methane-hydrogen with hydrogen-levels up to 80% by volume has been conducted in a swirl stabilized premixed combustor. Stereo particle image velocimetry (PIV) and OH* chemiluminescence imaging have been used in this study. Results show that there is a single-ringed structure of internal recirculation zone (IRZ) in the non-reacting flow, while in the reacting flows there is a complicated flow pattern with a two-celled IRZ structure in which the axial velocity near the center-axis is oriented downstream. As equivalence ratio decreases, the width of IRZ decreases in methane flames while it increases in hydrogen enriched flames, and the flame shape changes from conical to an elongated columnar shape, especially in hydrogen enriched flames. There are two different modes of vortex breakdown observed, spiral mode in methane flames and bubble mode in hydrogen enriched flames. The mechanisms of LBO in pure methane and hydrogen enriched premixed flames are shown to be different and explained in the present study.

INTRODUCTION

Modern premixed gas turbine combustors are usually operated at lean operating conditions for lowering combustion temperature and reducing the production rate of NOx [1-2]. The operation near the lean blowout limit, however, may induce undesirable combustion characteristics, such as flashback and acoustic combustion instabilities caused by local flame extinction and heat release fluctuation, leading to poor combustion efficiency and poor operability of the combustor. The heat release fluctuations when appropriately coupled with the acoustics can lead to large pressure and velocity fluctuations near the dump plane, with the latter serving as a precursor to flashback especially with fuels associated with higher flame speeds such as hydrogen. It is therefore of interest to better understand the combustion characteristics close to LBO limit.

Over the past several decades, extensive numerical and experimental studies on LBO phenomena have been conducted, including LBO observations characterized by large scale unsteadiness, local extinction and re-ignition [3-8]. LBO scaling as a function of combustion parameters (incoming flow velocity, equivalence ratio, pressure, temperature and fuel type) have been reported for specific combustor configurations [9-14], and active or passive control strategies have been explored [8, 15-18]. Several LBO mechanisms have been proposed, and include: balance between the rate of entrainment of reactants into the recirculation zone and the rate of burning[19], energy balance between heat supplied by the hot recirculating flow to the fresh gases and that released by reaction [20-23], balance between contact time between the combustible mixture and hot gases in the shear layer and chemical ignition time [20, 24-26], and mechanisms related to local extinction by excessive flame stretch with a flamelet based description [27-29]. In addition, it is believed that flame front instabilities play important roles in the blowout process in view of the reported observations of flame pulsating and flickering before the flow actually blows out [30, 31]. However, definitive conclusions on LBO remain a key challenge and need further investigation [29, 32]. This is particularly true for blended fuels such as Syngas where hydrogen is often present along with carbon monoxide, methane and other gases.

It is widely accepted that both flow behavior and chemical kinetics play a role in the LBO, but their relative roles on this phenomenon need further clarification. Moreover, it should be emphasized that the flame front involves key issues such as flame-vortex interaction, flame-wrinkling, flame holding and their relations to the flow field and turbulence levels. In addition, Zhang et al [33] observed that the averaged flow field structure did not change with a fixed adiabatic temperature for a methane flame, or flames with 20%, 50%, and 75% H_2. This indicates chemical kinetics does not affect the flow field structure. In a bluff body stabilized premixed flame, however, it has been reported that near blowoff the structure of reacting flow field appears to be changed back to the sinuous structure observed in non-reacting flow, randomly oscillating between a spatially well-organized sinuous flow structure and something more symmetric [29]. This observation implies that we cannot simply attribute LBO to a decreasing temperature ratio as equivalence ratio decreases.

Hydrogen has a wide flammability range, low minimum ignition energy, and high flame speed. Therefore, hydrogen enriched fuel has the benefit of extended lean flammability limits that allows stable ultra-lean combustion at lower temperatures needed to minimize the NOx production without any adverse effect on the combustion emissions of CO and unburned hydrocarbons (UHC). It may be assumed that the higher combustibility of the added hydrogen may increase NOx emission due to higher flame temperature (at a constant equivalence ratio), but this fact could be offset by the ability to burn an overall leaner mixture [34-37] so that lower thermal NOx is produced. However there are also several challenges with hydrogen addition. The main challenge is the susceptibility to flashback due to increased flame speeds associated with hydrogen content. For example, the flame speed of a stoichiometric methane air mixture is about 40 cm/s whereas that of a hydrogen air flame is about 210 cm/s at 1atm and room temperature [38]. This mismatch between flame speeds leads to flame holding problems in a gas turbine engine environment. Additionally, in a lean flame, the preferential diffusion instability associated with hydrogen content will trigger the flame front instabilities, and cause it to be more wrinkled and convolved. This thermo-diffusive instability is also likely to play a role in the LBO. Since hydrogen addition is likely to improve the LBO limit [14, 33, 39], but with added complexities of flashback, increased flame-wrinkling etc, it is important to understand the controlling mechanisms associated with LBO in hydrogen enriched flames. This need serves as the primary motivation for the present study.

In this study, the main goal is to expand the knowledge base concerning the fundamental controlling processes associated with LBO in hydrogen-enriched premixed combustion. This is done by investigating the flow field, the reaction zone, and the flame structure properties as flame approaches the LBO limit. Since the flame instabilities in the blowout process are very sensitive to external disturbance, 2D-PIV of a non-intrusive and laser-based diagnostic technique for velocity measurements and imaging of OH* chemiluminescence were used to capture the information regarding the flow field, reaction zone and flow-flame interaction as the blowout limit is approached. This data is then analyzed to generate some key mechanistic conclusions about LBO in hydrogen-enriched flames.

EXPERIMENTAL SETUP

Experiments at atmospheric pressure and room temperature have been conducted in an unconfined swirl stabilized combustor. Figure 1 shows the schematic of the experimental setup. The measurement system includes a 2D-PIV system for velocity measurement, and a high speed camera (Photron SA-3) for OH*-emissions measurement. The combustor consists of the inlet fuel and air-delivery system, and the premixing section. The flame is swirl-stabilized and attached to the center body at the dump plane for conditions corresponding to the measurements in this study.

As shown in Figure 2, a 45^0 swirl vane is fitted with a hollow center body. This center body extends beyond the swirl vane and is flush with the dump plane of the combustor. The exit diameter of the center body is 25.4 mm (1.0 inch) and the O.D. of the swirler is 34.9 mm (1.375 inch). The geometric swirl number is calculated to be S_g=0.76. Methane or hydrogen-enriched fuel mixture, and the air are injected radially into the annular air-fuel delivery system, 533 mm (21 inch) upstream of the dump plane, to ensure fuel and air is well premixed. The test matrix, in terms of equivalence ratio, is listed in Table 1, with all data taken at a Reynolds number of 17,670 based on the bulk velocity. For hydrogen-enriched methane mixture, the global equivalence ratio is calculated based on the ratio of stoichiometric air to fuel ratio (AFR) to actual AFR with blended methane and hydrogen. The hydrogen blend is expressed in the results as a volume percentage.

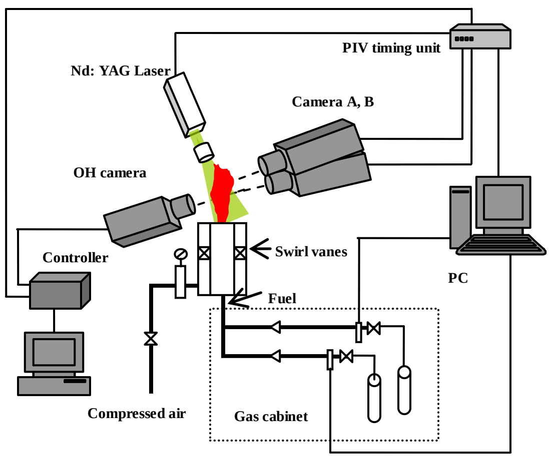

Figure 1. Schematic view of experimental set up.

For the 2D velocity measurements, a commercial PIV system (IDT Inc) is used, and in order to capture a large field of view without reducing the measure resolution, two cameras (SharpVision 1400DE) are used together as shown in Figure 1, where the two cameras are aligned vertically. The image data sets are processed separately and eventually combined together to yield a larger measurement domain. These CCD cameras have a resolution of 1360(H) ×1024(V) pixels with pixel size of 4.65 ×4.65 μm^2. Both cameras are equipped with Nikon lens of 50mm focal length. To illuminate the flow field of interest, laser-light from a twin head dual cavity Nd: YAG laser are combined and frequency doubled to generate two green light pulses at 532 nm, with pulse energy of 120 mJ and pulse duration of 5 ns. The laser beam, with diameter of 5 mm, goes through the optics of a cylindrical and a spherical lens and forms a light sheet of approximately 1.0 mm thickness in the measurement field. During the measurement, the PIV system is operated at a frame-pair rate of 5 Hz. The time delay between two laser pulses is between 15 and 20 µs, depending on the flow velocity; this time increment is used to optimize the accuracy of data processing. The field of view (FOV) of each camera is approximately 65mm×50mm, yielding the combined measurement domain of 65mm×85mm (including an overlap region). The seeding particles are required to be small enough to ensure good tracking of the fluid motion (Stokes number < 1) and big enough to scatter light for image capturing (also be resistant to high temperature). Here Al_2O_3 particles with nominal diameter of 1 µm are introduced upstream of the swirler in order to distribute them homogenously and to follow the flow oscillation with a frequency up to 10 KHz [40]. Although the PIV measurements do not resolve the 10 KHz time scale, it is important for the seeding particles to correctly represent the instantaneous fluctuations of the flow-field.

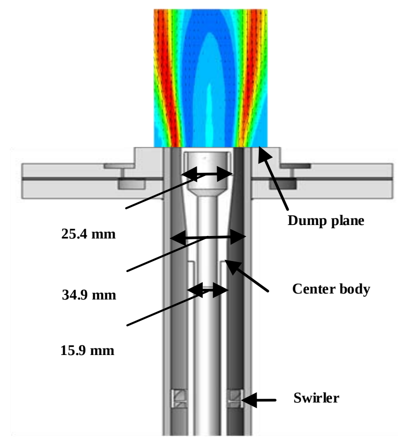

Figure 2. Sectional view of the swirl injector.

The IDT pro-VISION software was used to analyze the PIV data, and the adaptive interrogation mode was used since it provides a second-order accurate mesh free algorithm [41]. The measured 81×62 velocity vectors have a spatial resolution of approximately 0.8×0.7 mm. A total of 500 image pairs were usually recorded for each data set and statistically processed for the mean and RMS values. Considering a typical value in the measurement error of 0.1 pixel units [42], which combines bias and RMS errors, and a typical displacement of 8 pixel units in this experimental PIV measurement, this error is 1.25% of the mean local velocity.

Table 1. Experimental test matrix (hydrogen percentage based on volume basis)

Fuel	Φ_{LBO}	Φ_1	Φ_2	Φ_3	Φ_4
CH_4	0.675	0.744	0.694	0.689	0.684
40%H_2	0.450	0.669	0.474	0.464	0.457
60%H_2	0.345	0.654	0.447	0.359	0.354
80%H_2	0.255	0.432	0.340	0.268	0.264

Since OH* radicals are produced at the flame front and abundantly present in the reaction zone, OH* chemiluminescence imaging phase-locked with the PIV measurements has been carried out to investigate the instantaneous distribution of reaction zones, by using a high speed camera mounted with an achromatic ultraviolet lens (Nikkor, Inc) of 105-mm focal length and f/#4.5, and UV intensifier (Invisible Vision Ltd. Model number 1850-10) with frame rate of 2000 Hz and 10 images per each PIV triggering signal. The collected radiation of OH* first passes through an interference filter, centered at 308 nm and with a full-width-half-maximum (FWHM) of 10 nm, which corresponds to the primary spectral region for the OH to $A^2\Sigma^+$-$X^2\prod$ electronic transition.

RESULTS AND DISCUSSION

In presenting the results, we will discuss the flowfield behavior first and then examine the high speed chemiluminescence images to correlate the heat release behavior with the flow dynamics. The methane-only results will be contrasted with the data representing different hydrogen contents. We will conclude with an assessment of the LBO mechanisms for methane only and hydrogen enriched flames.

Flow field

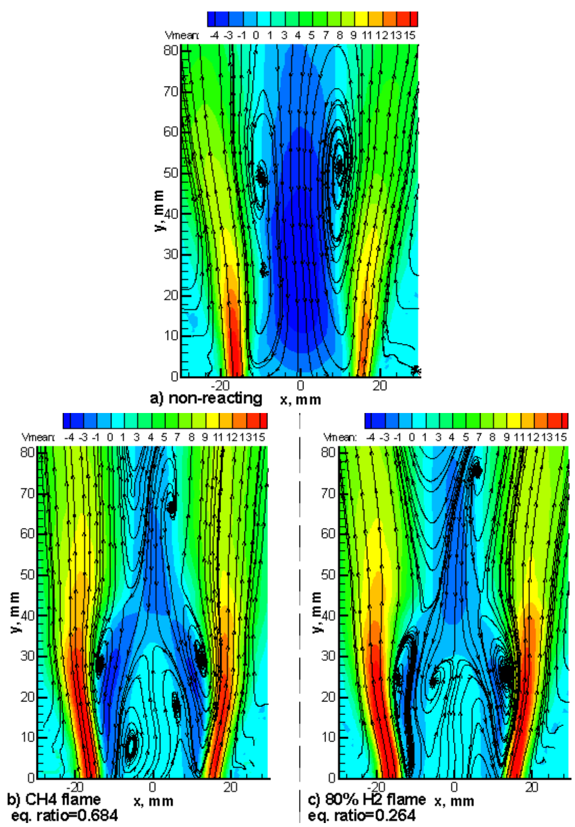

Figure 3. Axial velocity field for (a) non-reacting flow, (b) CH_4 flame at Φ=0.684 , and (c) 80% Hydrogen enriched flame at Φ=0.264.

Figure 3 show the contours of mean axial velocity V_{mean} for the non-reacting flow and for the reacting cases of methane-only and 80% hydrogen enriched flames, superimposed with corresponding streamlines. In the non-reacting flow, represented only by the swirling air flow, it is clearly seen that a pair of nearly axisymmetric recirculation zones are established above the dump plane, centered at nearly y/D=1.4 (y≈50mm), along with two weak corner recirculation zones. In the reacting flow with methane or 80% hydrogen enriched flames, a more complicated flow pattern is formed, with a two-celled structure in the interior of the recirculation zone (IRZ) and velocities near the flow centerline orientied downstream close to the dump plane, as also observed by Faler and Leibovich [43]. Compared to the single ring shape structure of internal recirculation zones in the non-reacting flow, two outer rings in the two-celled structure are observed adjacent to the IRZ and displaced upstream, positioned at nearly y/D=0.86 (y≈30mm). All reaction cases in this study have similar flow patterns.

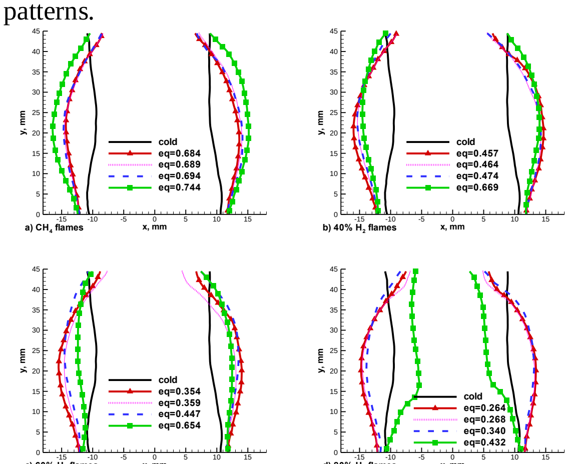

Figure 4. Boundaries of IRZ for (a) CH_4 flames, (b) 40% H_2 flames, (c) 60% H_2flames, and (d) 80% H_2 flames.

Figure 4 shows the boundaries of IRZ in cases of the methane flame, and the blended flames with 40%, 60%, and 80% hydrogen respectively, along with those in the non-reacting flow. In all the reacting cases, there was no flashback observed, and so changes in the observed flow patterns are not related to any flashback mechanism. The IRZ boundaries are obtained directly from the PIV measurements. The width of internal recirculation zones in the non-reacting flow initially increased immediately after the dump plane, and then decreased slightly, followed by an increase along the axis direction. The IRZ closes further downstream (beyond the axial region shown). This initial non-monotonic behavior is believed to be due to the effects of the center-body and the swirling flow. Very close to the dump plane, the recirculation mainly results from center-body effect. The region above the center-body creates a negative pressure gradient along the axis, and in turn, leads to the back-flow. Farther from the dump plane, the negative pressure gradient caused by the suction coefficient of center-body is mitigated and the width of recirculation reduced. Further downstream, the effect of the swirl generated upstream by a swirler dominates. The decay of the tangential velocity of the swirling flow induces another negative pressure gradient in the axis direction and increases the size of the recirculation zones. For all the reacting cases the width of the IRZ initially expands and then decays due to reduction of the tangential velocity (except the one corresponding to 80% H_2 equivalence ratio of 0.432). This behavior is believed to be more associated with the increased vorticity resulting from combustion-induced vorticity generation. Along the axial direction, the recovery of adverse pressure gradient caused by center-body was compensated for much earlier by the negative pressure gradient resulting from swirling effect, and the initial decay in the IRZ was not observed.

In addition, as shown in figure 4, in the case of hydrogen enriched flames, the width of IRZ increases as the equivalence ratio Φ is reduced. This behavior is mainly associated with the reduced axial velocities and increased local swirl level when Φ decreases. The increased swirl leads to a broadened width of the IRZ with reduced Φ. However the width of IRZ in the methane flame surprisingly decreases as the LBO limit is approached. This behavior is counter to the observation for the hydrogen enriched flames noted above and points to the existence of different LBO behavior for the two cases. As will be discussed, our observations indicate that there are two different modes of swirl-induced vortex breakdown for methane and hydrogen enriched flames.

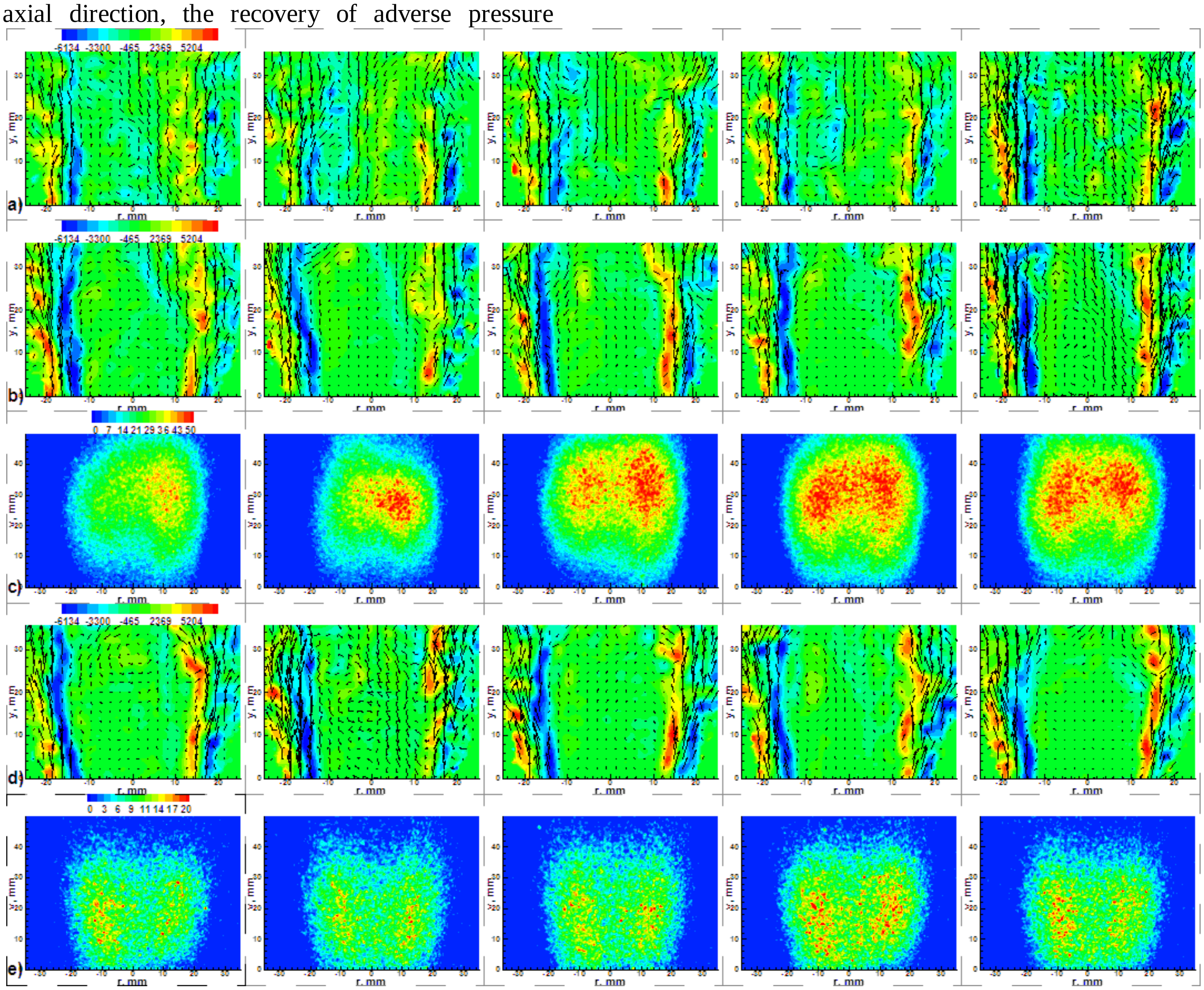

Figure 5. Instantaneous vorticity distributions for (a) non-reacting flow, (b) CH_4 flame at Φ=0.684, (d) 80% H_2 flame at Φ=0.264; and instantaneous OH* distributions for (c) CH_4 flame at Φ=0.684 and (e) 80% H_2 flame at Φ=0.264. Time increases from left to right with step increments of 0.2s.

Figure 5 shows the instantaneous vorticity distributions of non-reacting, methane flame (Φ=0.684), and 80% hydrogen enriched flame (Φ=0.264) with corresponding OH* signals. In both cases the flame is close to LBO. The superimposed velocity vectors are shown for every fourth time instance. From the time series of instantaneous vorticity maps at the time step increments of 0.2 second, the vorticity distribution along the flame front (annular shear layer) can clearly be visualized. It can be clearly seen that the vorticity levels associated with the reacting flows are higher and is related to the combustion-generated vorticity.

Figure 5c and 5e show the instantaneous OH* distributions for the two flames and point to key differences. In fig. 5c, for methane, the flame near LBO is lifted from the dump plane and shows variation in size with time. This is characteristic of a precessing vortex core (PVC) that is generally sensitive to external perturbation [44]. For the hydrogen flame in fig.5e, the OH* distributions are anchored closer to the dump plane. Further, the flame is thermo-diffusively stable for methane fuel with corresponding Lewis number of about unity, while it is thermo-diffusively unstable for lean hydrogen fuel with corresponding Lewis number less than unity due to its preferential diffusivity. As will be discussed later, the different OH* behavior for the methane flame and the hydrogen flame near LBO are related to different modes of instability of vortex breakdown. Thus, in methane flames with PVC, as equivalence ratio decreases, the heat release and flow dilatation decrease, leading to reduced vortex strength. The vortex is in opposite sense to the swirling flow and induces adverse pressure gradient in the axis direction, and is responsible for the decreased width of IRZ. In hydrogen enriched flames, the flame front instability causes the oscillation of reacting fronts to be greater temporally and spatially, and leads to the amplified width of the IRZ as the LBO limit is approached.

In order to verify the occurrence of PVC, a high speed measurement of OH* signal was carried out in a region spanning y from 17 mm to 52 mm, and x from -40 mm to 25 mm, as shown by the large rectangle in figure 6. Gate time and framing rate were set at 90 μs and 10K fps, respectively. The signal was recorded for 2.1 seconds. A total of six different locations, with x steps of 15 mm and y steps of 10 mm, were processed and shown as points A-F in figure 6, and two different calculation spot sizes of 1x1 mm^2 and 5x5 mm^2 were used to do the spectral analysis. It is found that neither location nor spot size affects the calculated spectral results. Figure 7 shows the power spectrum plots of OH* signal frequency in methane flames and 80% hydrogen enriched flames, obtained at point F (-15mm, 30mm) and with calculation spot size of 1x1 mm^2. Figure 7a shows that all three measured methane flames of equivalence ratios of 0.684, 0.694 and 0.744 have strong spectra, located at 22 Hz, 89 Hz and 77 Hz, respectively. The maximum Strouhal number obtained from the spectral analysis is of the order of 0.05 which is much smaller than a jet-vortex shedding frequency for which Strouhal numbers in the range of 0.2-0.3 are expected. The periodic unsteadiness for the methane flame is therefore associated with the PVC. Clearly as LBO is approached, the PVC frequency decreases and is related to the PVC breakdown preceding LBO.

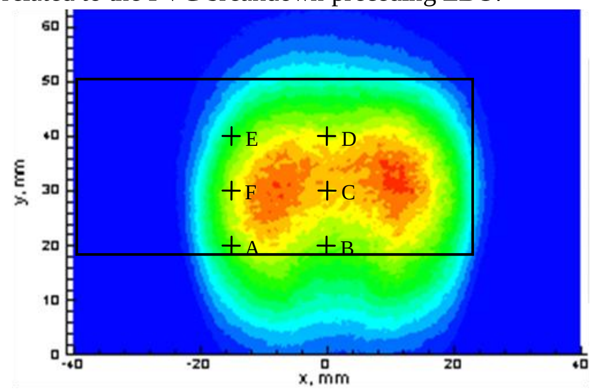

Figure 6. OH* spectral measurement points.

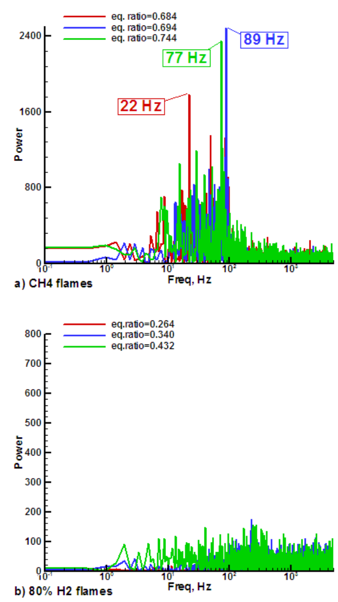

Figure 7. Power spectra of OH* signal for (a) CH_4 flames, and (b) 80% H_2 enriched flames.

In figure 7b, for 80% hydrogen enriched flames, a peak frequency in the spectrum is not obtained. Similarly, there is no evidence of a spectrum peak observed in the 40% or 60% hydrogen enriched flames. These results indicate broad-band unsteadiness absent of any PVC observed for the methane flame. This indicates that hydrogen addition mitigates the PVC behavior observed for methane flames.

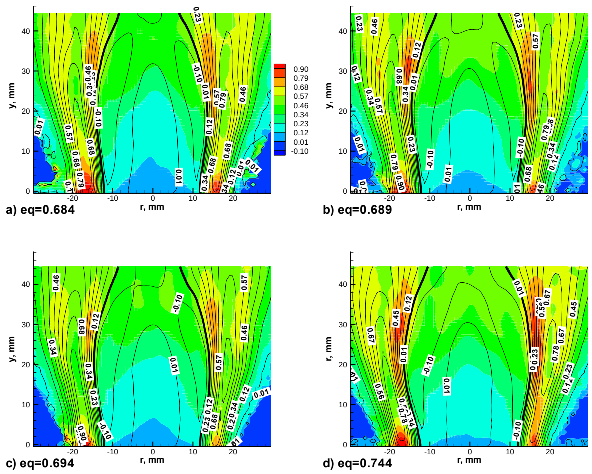

Figure 8. Normalized V_{rms} color contour superimposed with normalized V_{mean} line contour and thickened IRZ lines for CH_4 flames for a) Φ=0.684, b) Φ=0.689, c) Φ=0.694, and d) Φ=0.774.

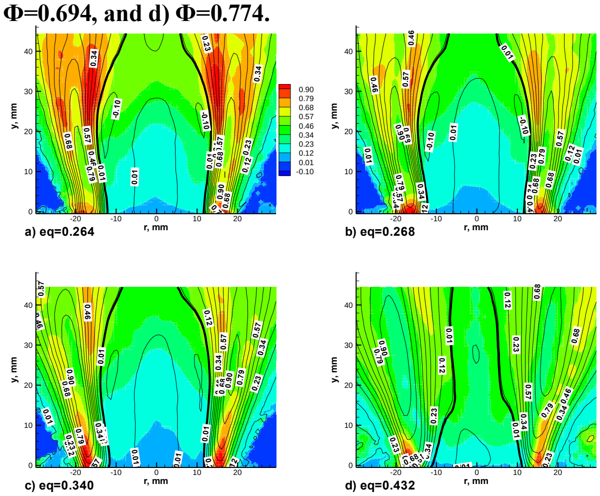

Figure 9. Normalized V_{rms} color contour superimposed with normalized V_{mean} line contour and thickened IRZ lines for 80% H2 flames for a) Φ=0.264, b) Φ=0.268, c) Φ=0.340, and d) Φ=0.432.

Figure 8 and 9 show the color contours for axial velocity RMS superimposed with line contours for axial velocities and thick-black lines representing the envelope of IRZ in methane flames, and in the 80% hydrogen enriched flames, respectively. Both axial velocities and their RMS are normalized with their corresponding maximum values in each case, in order to compare the distribution pattern of axial velocity fluctuation. For methane flames, as equivalence ratio decreases, the axial velocity fluctuation concentrated in inner shear layer in figure 8d is spread out and becomes more homogeneous in inner and outer shear layers in figure 8a. For 80% hydrogen enriched flames, however, approaching LBO limit, the distribution of axial velocity fluctuation is spatially more concentrated as shown in figure 9a and 9d. The 40% and 60% H_2 mixture cases have a similar pattern and trend as the 80% H_2 case and are not shown here.

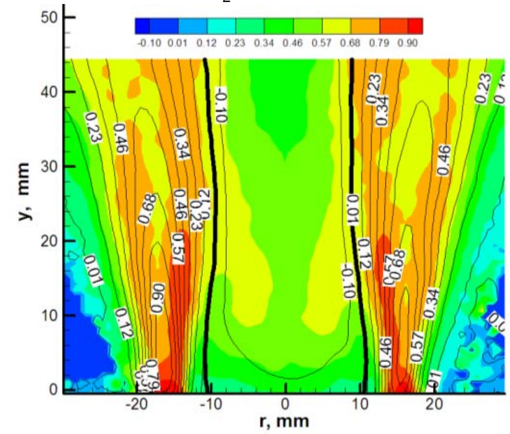

Figure 10. Normalized V_{rms} color contour superimposed with normalized V_{mean} line contour and thickened IRZ lines for non-reacting flow.

The observed differences in changes of the axial velocity fluctuation approaching the LBO limit are believed to be resulting from different controlling processes of LBO in methane flames and hydrogen enriched flames, respectively. It is noted that, as shown in figure 10, peaks of axial velocity RMS in non-reacting case are closer to the zero stream-function (outside the IRZ) due to shear layer generated turbulence. Further, the axial velocity RMS decreases downstream and toward the boundary of IRZ because of the dissipation. Considering that the reaction takes place in the shear layer between the high velocity annular shear layer and the IRZ, as shown in next section (figure 11-14), there are two paths for flames to advance toward a favorable reaction region of lower turbulence levels-downstream and inward toward the IRZ. As shown in the OH* contours in figure 11, when equivalence ratio deceases, the flame fronts for methane flames moves toward the envelope of IRZ of non-reacting flow (the width of IRZ in CH_4 flames decreases toward LBO), and moves downstream. Reaction takes place in the shear layer and within the IRZ, so a more homogeneous distribution of axial velocity RMS is formed. In hydrogen enriched flames, however, the flame fronts and the IRZ approach each other (the width of IRZ in H_2 enriched flames increases toward LBO) toward LBO, and the combustion can even reside within the IRZ (e.g. in figure 14d) almost completely, leading to combustion generated turbulence that is more concentrated.

Reaction dynamics

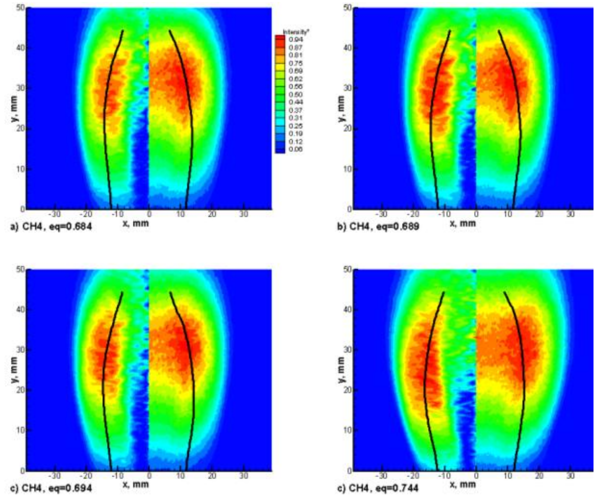

Figure 11. Abel inverted (LHS) and global (RHS) distributions of averaged OH* superimposed with IRZ lines for methane flames for a) Φ=0.684, b) Φ=0.689, c) Φ=0.694, and d) Φ=0.744.

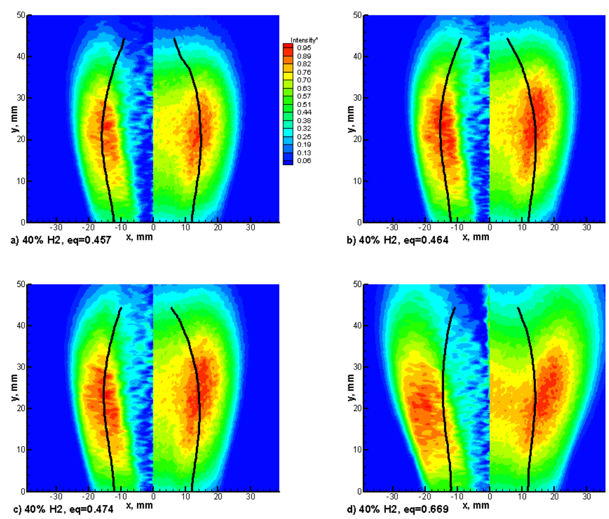

Figure 12. Abel inverted (LHS) and global (RHS) distributions of averaged OH* superimposed with IRZ lines for 40% hydrogen flames for a) Φ=0.457, b) Φ=0.464, c) Φ=0.474, and d) Φ=0.669.

In each flame, a total number of 1250 OH* images were captured. For every data set, each image was first corrected by the background image, then filtered and averaged over the whole sequence of 1250 images to yield the mean line-of-sight OH* image. This averaged global OH* image was then numerically Abel inverted to unfold the radial distribution of OH* signal by using Nestor-Olsen algorithm, which transforms the Abel inversion equation into a summation to allow processing of discrete sets of data and is widely employed due to its easy computation with reasonable accuracy [45-47]. Figure 11-14 show the Abel inverted radial (LHS) and line-of-sight global (RHS) distributions of the background-corrected OH* intensity averaged over 1250 images, superimposed with corresponding boundaries of IRZ represented by the thickened black lines, for pure methane, 40%, 60%, and 80% hydrogen enriched flames, respectively. The OH* intensities have been normalized by individual intensity maximum. In figure 11, for methane flames, as equivalence ratio decreases from 0.744 to 0.684, the center of reaction zone (OH*) moves radially inward from 16mm to 12mm approximately, and downstream from 25mm to 30 mm. For the 80% hydrogen enriched flame in figure 14, when Φ is decreased from 0.432 to 0.264, the center location of reaction zone also moves radially inward from 17 mm to 12mm, but does not change axially, located around 16mm at all times. As Φ decreases, the reaction in hydrogen enriched flames takes place almost completely within the IRZ, where hot combustion product is pulled back and the residential time is longer, providing a favorable combustion environment. Furthermore, the flame shape changes from a conical to a more elongated columnar shape as the equivalence ratio is reduced, especially in hydrogen enriched flames, leading to stronger interaction between the flame and the flow.

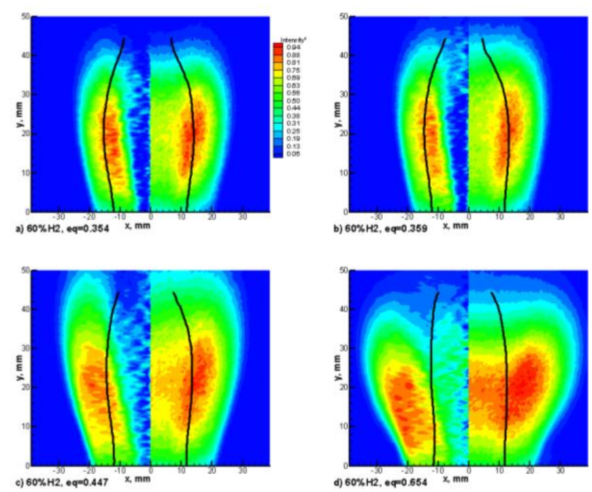

Figure 13. Abel inverted (LHS) and global (RHS) distributions of averaged OH* superimposed with IRZ lines for 60% H2 enriched flames for a) Φ=0.354, b) Φ=0.359, c) Φ=0.447, and d) Φ=0. 654.

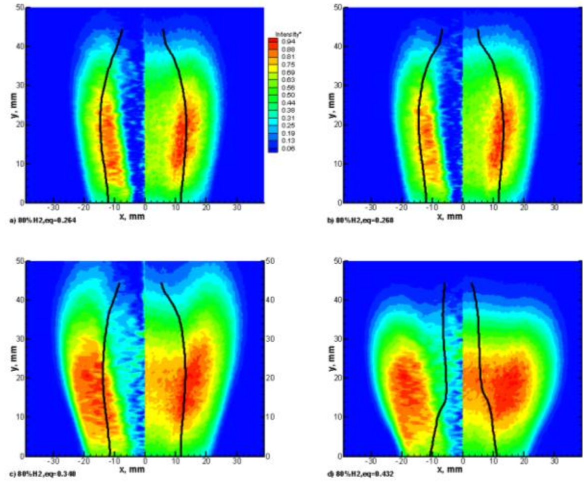

Figure 14. Abel inverted (LHS) and global (RHS) distributions of averaged OH* superimposed with IRZ lines for 80% hydrogen enriched flames for a) Φ=0.264, b) Φ=0.268, c) Φ=0.340, and d) Φ=0.432.

LBO Mechanism

Based on the measurement of the reaction zones and the flow field, a LBO mechanism is proposed and described in figure 15. The basic process of LBO is as follows: as equivalence ratio reduces, the flame resistance to turbulence and stretch is reduced and flame quenching occurs locally. The flame moves to the region of lower turbulence level and toward the boundary of IRZ (OH* maxima closer to IRZ is observed). Some unburnt mixture is entrained into IRZ via the rear of the toroidal vortex and burns within IRZ where hot combustion product is present and the residential time is longer. This process, in turn, can re-ignite the locally extinguished flame in the shear layer close to IRZ. As the equivalence ratio is further reduced, the reaction within IRZ fails to survive, leading to the final LBO. Specifically, for methane flames, with PVC and a Lewis number around one, the reaction of entrained unburnt methane mixture inside the IRZ is hindered by the decreased width of the IRZ, leading to reactions that occur mostly in the shear layer; the reduced flame speed leads to the flame moving downstream convectively (OH* maxima moved downstream observed) as the LBO limit is approached. In hydrogen enriched flames, with Lewis number less than one, the locally available and excess reactant of hydrogen with high mass diffusivity in the shear layer diffuses more rapidly into the IRZ with locally deficient reactant but favorable combustion environment. The molecular diffusion is more rapid than the thermal diffusion from IRZ that compensates for the heat loss by local flame quenching (almost constant axial location of OH* maxima observed). The unburnt reactants are burning immediately within IRZ with the help of longer contact time with hot products and increased width of IRZ. This reaction within IRZ, functioning as a small pilot flame, may not be able to ignite the flame in the shear layer but can sustain itself within IRZ as equivalence ratio is further decreased. The LBO happens after this flame kernel fails to survive itself, with the flame-flow interaction resulting in an elongated columnar shape flame from conical shape.

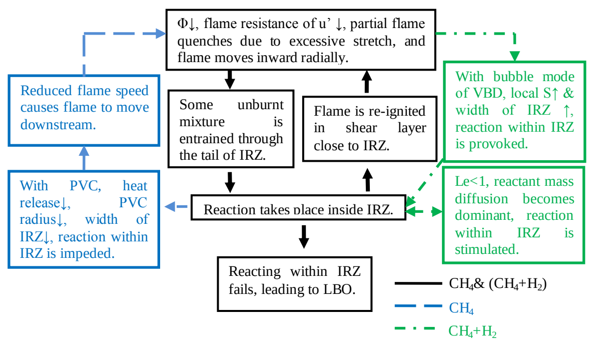

Figure 15. Hypothesis diagram for LBO mechanisms of methane and hydrogen enriched flames.

CONCLUSION

An experimental study was performed in a swirl stabilized combustor with the goal of understanding the flame behavior as the equivalence ratio was decreased toward LBO. Fuels used were pure methane, and methane blended with 40%, 60%, and 80% hydrogen. The following major conclusions are made.

1) Both the center-body and swirl level affect the central recirculation zone. The near field above the center-body is dominated by the center-body, while the far field is influenced by the swirl.
2) Combustion forces the stagnation point of vortex breakdown to move upstream, and generates a more complicated two-cell flow pattern where the center-line axial velocity near the dump plane is oriented downstream. In comparison, for the non-reacting flow a symmetric vortex structure is observed where the axial velocity near the axis is oriented upstream.
3) As the equivalence ratio approaches the LBO limit, the width of IRZ in the methane-only flame decreases, while that in the hydrogen-enriched flame increases. The PIV measurement and OH* spectral measurement show that the vortex breakdown is in a spiral mode (PVC) in the methane flame while a bubble type vortex breakdown is observed in the hydrogen-

enriched flames. It is believed that the flame front instability associated with the preferential diffusivity of the hydrogen content transitions the PVC into a more stable bubble type of vortex breakdown.

4) For methane flames, approaching the LBO limit, the reaction zone is moved inward toward the IRZ, and convectively moved downstream. The decreased width of the IRZ serves as a barrier to burn methane under much leaner conditions, compared to the hydrogen enriched flames with a larger IRZ.
5) For hydrogen enriched flame, as equivalence ratio decreases and LBO limit is approached, the excess reactant with the high mass diffusivity hydrogen content in the shear layer (resulting from local flame quenching) diffuses more rapidly into the IRZ with locally deficient-reactant but favorable combustion environment. Reactions take place within the IRZ with the help of longer residence times, and serves as a pilot flame to re-ignite any quenched flame in the shear layer. In addition, the increased width of IRZ approaching LBO limit favors reactions to be within and mostly within the IRZ, so that leaner flame can be sustained. As equivalence ratio is further decreased, this flame kernel in the IRZ is not able to ignite the flame in the shear layer but can sustain itself within the IRZ.

ACKNOWLEDGEMENTS

Authors would like to express their gratitude for the support obtained from Louisiana Board of Regents-Clean Power and Energy Research Consortium (CPERC). Support to CPERC from the Department of Energy is acknowledged.

REFERENCES

[1] C.K. Westbrook and F.L. Dryer, “Chemical kinetic modeling of hydrocarbon combustion”, Prog. Energy Combustion Science, 10 (1984)1-57

[2] V.L. Zimont, “The theory of turbulent combustion at high Reynolds numbers”, Combustion Explosions and Shock Waves, 15(1979)305-311

[3]Y.C. Chao, Y.L. Chang, C.Y. Wu, and T.S. Cheng, “An experimental investigation of the blowout process of a jet flame”, Proc. Comb. Inst., Vol. 28, 2000

[4] H. Nicholson and J. Field, “Some experimental techniques for the investigation of mechanism of flame stabilization in the wakes of bluff bodies”, Proc. Comb. Inst., Vol. 3, 1951, pp. 44-68

[5] S.R.N. De Zilwa, J.H. Uhm, and J.H. Whitelaw, “Combustion oscillations close to the lean flammability limit”, Comb. Sci. and Technol., Vol. 160, 2000, pp 231-258

[6] T. M. Muruganandam, S. Nair, Y. Neumeier, T. Lieuwen, and J. M. Seitzman, “Optical and acoustic sensing of lean blowout precursors”, 38th AIAA/ASME/SAE/ASEE Joint Propulsion Conference & Exhibit July 7-10, 2002,Indianapolis, Indiana, AIAA 2002-3732

[7] S. Nair and T. Lieuwen, “Acoustic detection of blowout in premixed flames”, J. Prop. Power, 21 (1) (2005) 32–39.

[8] M. Thiruchengode, S. Nair, S. Prakash, D. Scarborough, Y. Neumeier, T. Lieuwen, J. Jagoda, J. Seitzman, and B. Zinn, “An active control system for LBO margin reduction in turbine engines”, AIAA 2003–1008, Forty-first AIAA Aerospace Sciences Meeting and Exhibit, Reno, NV, January 6–9, 2003.

[9] E.E. Zukoski and F.E. Marble, “Experiments concerning the mechanism of flame blowoff form bluff bodies”, Proceedings of the Gas Dynamics Symposium on Aerothermochemistry, 1956. Northwestern University, Evanston, Illinois.

[10] E.E. Zukoski, and F.E. Marble, “The role of wake transition in the process of flame stabilization on bluff bodies”, AGARD Combustion Researches and Reviews, 1955:p. 167-180

[11] C.R. King, “Experimental investigation of effects of combustion chamber length and inlet total temperature, total pressure, and velocity on afterburner performance”, NACA RM E57C07, National advisory committee on aeronautics, 1957.

[12] H.C. Hottel, G.C. Williams, W.P. Jensen, A.C. Tobey, and M.R. Burrage, “Modeling studies of baffle-type combustors”, Ninth Symposium (International) on Combustion. 1962. p. 923-935.

[13] I. Glassman, “Combustion”, Academic Press: New York, 1996.

[14] David R. Noble, Qingguo Zhang, Akbar Shareef, Jeremiah Tootle, Andrew Meyers, and Tim Lieuwen, “Syngas mixture composition effects upon flashback and blowout”, Proceedings of GT2006 ASME Turbo Expo 2006, Barcelona, Spain. GT2006-90470

[15]Hejie Li, Xin Zhou, Jay B. Jeffries, and Ronald K. Hanson, “Active control of lean blowout in a swirl-stabilized combustor using a tunable diode laser”, Proc. Combust. Inst., 31(2007) 3215-3223

[16] E. Gutmark, T.P. Parr, D.M. Hanson-Parr, and K.C. Schadow, “Use of chemiluminescence and neural networks in active combustion control”, Proceedings of the Combustion Institute, 23 (1990)1101–1106.

[17] G.J. Sturgess, S.P. Heneghan, M.D. Vangsness, D.R. Ballal, A.L. Lesmerises, and D. Shouse, “Effects of back-pressure in a lean blowout research

combustor", J. Eng. Gas Turb. Power 115 (1993) 486–498.
[18] M.D. Durbin and D.R. Ballal, "Studies of lean blowout in a step swirl combustor", J. Eng. Gas Turb. Power 118 (1996) 72–77
19] J.P. Longwell, "Flame stabilization by bluff bodies and turbulent flames in ducts", Proc. Combust. Inst. 4 (1953) 90–97.
[20] FA.Williams, "Flame stabilization of premixed turbulent gases", Applied Mechanics Surveys, 1966:1157–70
[21] GC Williams, HC Hottel, and AC Scurlock, "Flame stabilization and propagation in high velocity gas streams", Proceedings of the Combustion Institute, 1951: 21–40.
[22]KM Kundu, D Banerjee, and D.Bhaduri, "On flame stabilization by bluff-bodies", Journal of Engineering for Power 1980 (January):209–14.
[23] KM Kundu, D Banerjee, and D.Bhaduri, "Theoretical analysis on flame stabilization by a bluff-body", Combustion Science and Technology (1977)153–162.
[24] Zukoski EE, "Flame stabilization on bluff bodies at low and intermediate Reynolds numbers". PhD Thesis, California Institute of Technology, Pasadena,1954.
[25] DB Spalding, "Theoretical aspects of flame stabilization", Aircraft Engineering, (1953)264–276.
[26] EE Zukoski. In: Oates G, editor. Afterburners; 1997.
[27]S. Yamaguchi, N. Ohiwa, and T. Hasegawa, "Structure and blow-off mechanism of rod-stabilized premixed flame", Combust. Flame 62(1985) 31-41
[28]J.C. Pan, M.D. Vangsness, and D.R. Ballal, "Aerodynamics of bluff-body stabilized confined turbulent premixed flames", J. Eng. Gas Turb. Power (1992) 783-789
[29] Swetaprovo Chaudhuri, Stanislav Kostka, Michael W. Renfro, and Baki M. Cetegen , "Blowoff dynamics of bluff body stabilized turbulent premixed flames", Combustion and Flame 157 (2010) 790–802
[30] M. Füri, P. Papas, and P.A. Monkewitz, "Non-premixed jet flame pulsations near extinction", Proc. Combust. Inst. 28 (2000) 831–838.
[31] E.W. Christiansen, C.K. Law, and C.J. Sung, "The role of pulsating instability and global Lewis number on the flammability limit of lean heptane/air flames", Proc. Combust. Inst. 29 (2000) 807–814.
[32] S. Shanbhogue, S. Husain, and T. Lieuwen, "Lean blowoff of bluff body stabilized flames: Scaling and dynamics", Prog. Energy Combust. Sci. 35 (2009) 98–120.
[33] Qingguo Zhang, David R. Noble, Santosh J. Shanbhogue, and Tim Lieuwen, "Impacts of hydrogen addition on near- lean blowout dynamics in a swirling combustor", Proceedings of GT2007 ASME Turbo Expo 2007, Montreal, Canada, GT2007-27308
[34] E.R. Hawkes and J.H. Chen, "Direct numerical simulation of hydrogen-enriched lean premixed methane–air flames", Combustion and Flame 138 (2004), pp. 242–258.
[35] A.R. Choundhuri and S.R. Gollahalli, "Combustion characteristics of hydrogen–hydrocarbon hybrid fuels", Hydrogen Energy 25 (2000), pp. 451–462
[36] A.R. Choundhuri and S.R. Gollahalli, "Characteristics of hydrogen–hydrocarbon composite fuel turbulent jet flame", Hydrogen Energy 28 (2003), pp. 445–454
[37] G.A. Karim, I. Wierzba, and Y. Al-Alousi, "Methane–hydrogen mixture as fuels", Hydrogen Energy 21 (1996), pp. 625–631.
[38] Stephen R. Turns, "An introduction to combustion: concepts and applications", Second Edition, McGraw Hill Inc., 2000
[39] D. Littlejohn, and R.K. Cheng, "Fuel effects on a low-swirl injector for lean premixed gas turbines", Proceedings of the Combustion Institute 31 (2007) 3155–3162
[40] A Melling, "Tracer particles and seeding for particle image velocimetry", Meas. Sci. Technol. 8 (1997) 1406-1416
[41] L. M. Lourenco and A. Krothapalli, "True resolution PIV: a mesh-free second order accurate algorithm", Proceeding of the international conference on applications of laser fluid mechanics, Lisbon, 2000
[42]J. Westerweel, "Digital Particle Image Velocimetry-theory and application", Delft University Press, 1993
[43] JH Faler, and S.Leibovich, "Disrupted states of vortex flow and vortex breakdown", Phys Fluids 20(1977):1385-400
[44] N. Syned, A.K. Gupta, and J.M Beer, "Temperature and density gradients arising with the precessing vortex core and vortex breakdown in swirl burners", Proceedings of the 15th international symposium on combustion, (1975) 587-597
[45] O.H. Nestor, and H.N. Olsen, "Numerical methods for reducing line and surface probe data", SIAM Review, 2(3) (1960) 200-207.
[46] M.W. Blades, and G. Horlick, "Photodiode array measurement system for implementing Abel inversions on emission from an inductively coupled plasma", Appl. Spectrosc., 34(1980) 696-699
[47] U. Engel, C. Prokisch, E. Voges, G.M. Hieftje, and J.A.C. Broekaert, "Spatially Resolved Measurements and Plasma Tomography with Respect to the Rotational Temperatures for a Microwave Plasma Torch" , J. Anal. Atom. Spectrom., 13 (1998) 955-961.